



HAL
open science

Collapses, maxima, multi-year modulation and trends of the Zapiola Anticyclonic Circulation: insights from Mercator reanalysis

Lea Poli, Camila Artana, Christine Provost, Jérôme Sirven, Ruben Le Blanc-Pressenda

► To cite this version:

Lea Poli, Camila Artana, Christine Provost, Jérôme Sirven, Ruben Le Blanc-Pressenda. Collapses, maxima, multi-year modulation and trends of the Zapiola Anticyclonic Circulation: insights from Mercator reanalysis. *Journal of Geophysical Research. Oceans*, 2024, 129 (3), pp.e2023JC020269. 10.1029/2023jc020269 . hal-04546473

HAL Id: hal-04546473

<https://hal.science/hal-04546473v1>

Submitted on 16 Apr 2024

HAL is a multi-disciplinary open access archive for the deposit and dissemination of scientific research documents, whether they are published or not. The documents may come from teaching and research institutions in France or abroad, or from public or private research centers.

L'archive ouverte pluridisciplinaire **HAL**, est destinée au dépôt et à la diffusion de documents scientifiques de niveau recherche, publiés ou non, émanant des établissements d'enseignement et de recherche français ou étrangers, des laboratoires publics ou privés.



Distributed under a Creative Commons Attribution 4.0 International License

Collapses, Maxima, Multi-Year Modulation and Trends of the Zapiola Anticyclonic Circulation: Insights From Mercator Reanalysis

**Key Points:**

- The Zapiola circulation is bottom intensified and its volume transport ranges from -18.5 to 268 Sv with a mean of 122 Sv
- We analyze collapses, maxima, multi-year modulation and trends in the Zapiola transport and associated water characteristics variations
- In the last 27 years trends in the Zapiola region include transport reduction and increase in temperature and salinity in the upper $2,000$ m

Supporting Information:

Supporting Information may be found in the online version of this article.

Correspondence to:

L. Poli,
lea.poli@locean.ipsl.fr

Citation:

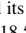

Poli, L., Artana, C., Provost, C., Sirven, J., & Le Blanc-Pressenda, R. (2024). Collapses, maxima, multi-year modulation and trends of the Zapiola Anticyclonic Circulation: Insights from Mercator reanalysis. *Journal of Geophysical Research: Oceans*, *129*, e2023JC020269. <https://doi.org/10.1029/2023JC020269>

Received 19 JULY 2023

Accepted 19 FEB 2024

Author Contributions:

Investigation: Lea Poli, Camila Artana, Christine Provost, Jérôme Sirven, Ruben Le Blanc-Pressenda

Lea Poli¹ , Camila Artana^{1,2} , Christine Provost¹, Jérôme Sirven¹, and Ruben Le Blanc-Pressenda¹

¹LOCEAN-IPSL, Sorbonne Université (UPMC), Paris, France, ²Institut de Ciències del Mar, Barcelona, Spain

Abstract The Argentine Basin hosts a unique oceanic feature: the Zapiola Anticyclonic Circulation (ZAC) located above a sedimentary deposit. Taking advantage of a high-resolution ($1/12^\circ$) global ocean reanalysis (GLORYS12) we examine the ZAC over 27 years (1993–2019). The mean ZAC is bottom-intensified with bottom currents reaching 0.10 ms^{-1} . The ZAC volume transport ranges from -18.5 to 268 Sv with a mean of 122 Sv. The strong negative peaks correspond to occasional ZAC collapses. During large transport events (>195.4 Sv) the ZAC shows a well defined coherent gyre. Strong transport events are associated with high eddy kinetic energy (EKE) at the periphery of the ZAC (especially to the west and south). In contrast, during weak transport events (<49.8 Sv), EKE increases at the center of the ZAC and decreases at the ZAC periphery. A weak ZAC is more permeable to external mesoscale structures. Each weak event features a cyclonic eddy at the center of the ZAC carrying subantarctic cold and fresh waters. The ZAC exhibits a multi-year modulation, with periods of 4–5 years (1993–1997, 1998–2003 and 2004–2009) of low salinity corresponding to low transport, and high salinity to high transport. Over the last 27 years, transport time series exhibit a significant negative trend of -15 $\text{Sv}\cdot\text{decade}^{-1}$ associated with a negative trend in EKE (-0.015 $(\text{m/s})^2\cdot\text{decade}^{-1}$) to the north west of the ZAC. Waters in the Zapiola region become warmer and saltier in the first $2,000$ m of the water column because of the southward migration of the subtropical front.

Plain Language Summary In the southwest Atlantic, the Argentine Basin hosts a unique oceanic feature: the Zapiola Anticyclonic Circulation located above a sedimentary deposit. The Zapiola Anticyclonic Circulation rotates counter-clockwise and has a mean transport comparable to those of the strongest ocean currents (122 million cubic meters per second). The Zapiola Anticyclonic Circulation undergoes extreme variations with collapses and intensifications reaching 300 million cubic meters per second. Episodes of weak Zapiola transport tend to occur in austral winter and episodes of strong transport in austral summer. The Zapiola Anticyclonic Circulation exhibits a multi-year modulation, with periods of 4–5 years (1993–1997, 1998–2003 and 2004–2009) of low salinity corresponding to low transport, and high salinity to high transport. Over the last 27 years, the Zapiola Anticyclonic Circulation transport diminished and waters in the region became warmer and saltier in the upper $2,000$ m of the water column.

1. Introduction

The Argentine Basin is one of the most energetic regions of the world ocean in terms of mean flow and mesoscale activity (Mason et al., 2017). The spatial distribution of surface Eddy Kinetic Energy (hereafter EKE) maxima forms a C-shape around a relative minimum (values lower than 0.01 m^2 s^{-2}) in the center of the basin (Figure 1). This minimum is associated with a particular oceanic feature, the Zapiola Anticyclonic Circulation (hereafter ZAC). The ZAC is located above a sedimentary deposit (the Zapiola Rise, centered at 45°W , 45°S).

The ZAC existence was first suggested from photographed mud waves (Flood & Shor, 1988). The current measurements that followed (Weatherly, 1993; Whitworth et al., 1991) supported the concept of an anticyclonic circulation. Subsequently, Saunders and King (1995) made the first measurements in the ZAC from a shipborne ADCP system and hydrographic measurements. They measured a synoptic intensified flow at depth and suggested the presence of a barotropic anticyclonic circulation with a transport equivalent to that of the strongest ocean currents (>100 Sv). Mean transport estimates were then produced and cover a wide range of values. A mean transport of 50 Sv was obtained using altimetry-derived surface geostrophic velocities over the period 1993–2007 under barotropic flow assumption (Saraceno et al., 2009). Colin de

© 2024 The Authors.

This is an open access article under the terms of the [Creative Commons Attribution-NonCommercial-NoDerivs License](#), which permits use and distribution in any medium, provided the original work is properly cited, the use is non-commercial and no modifications or adaptations are made.

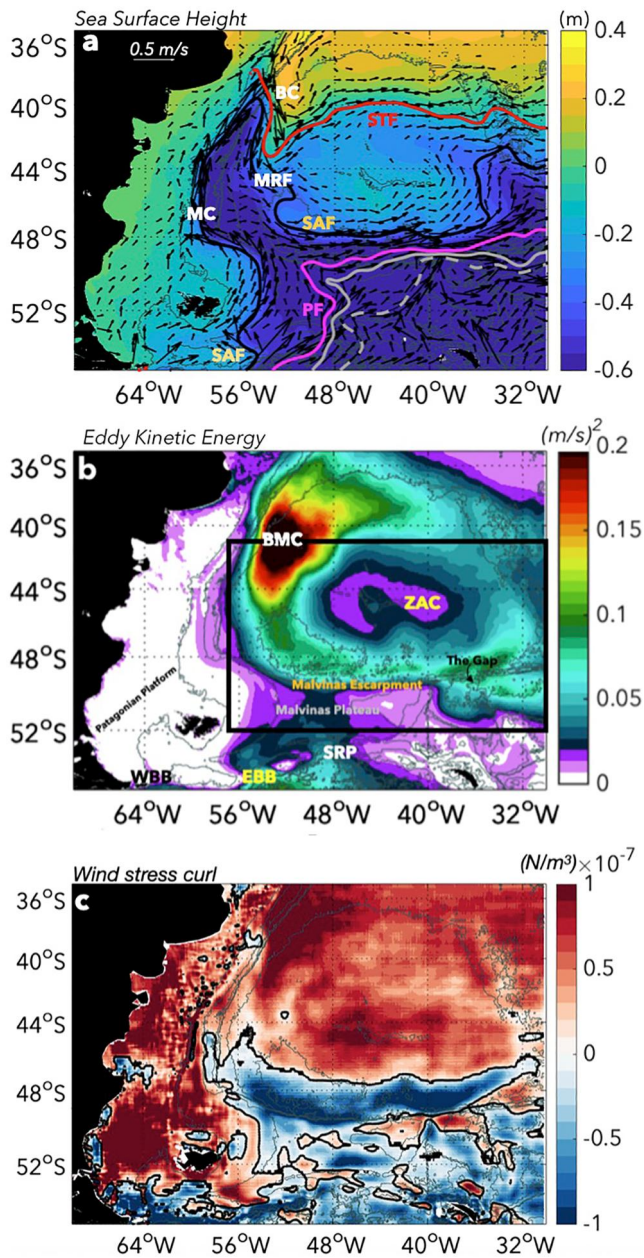


Figure 1. (a) Mean sea surface height (in m) and mean surface velocities (arrows). (b) Mean surface eddy kinetic energy. The fields from GLORYS12 reanalysis are averaged over 1993–2019 period. Sea surface height contours indicate the front positions in panel (a) Subantarctic Front (SAF, black isoline -0.38 m), Northern Polar Front (PF-N, magenta isoline -0.77 m), Main Polar Front (PF-M, thick gray isoline -0.91 m), Southern Polar Front (PF-S, dashed gray isoline -1.05 m) and Subtropical Front (STF, red isoline -0.13 m). In panel (b), EBB stands for East of Burdwood Bank, WBB for West of Burdwood Bank, SRP for Shag Rock Passage, Zapiola Anticyclonic Circulation (ZAC) and the Brazil-Malvinas Confluence (BMC). The black rectangle shows the region plotted in (c) and (d) in Figure 2. (c) Mean Wind Stress Curl from ERA-interim reanalysis averaged over the period 1993–2019.

Verdière and Ollitrault (2016) used an ocean climatology combined with 1,000-m Argo velocities to estimate the full-depth streamfunction over the period 2004–2010 which led to a larger mean transport of 124 Sv. Recently, Johnson and King (2023) estimated a mean ZAC transport of 110 Sv by referencing geostrophic shear from mean climatology (World Ocean Atlas 2018) to mean 1,000-dbar velocities that they estimated from Argo float displacements and highlighted the bottom-intensified nature of the ZAC.

According to theoretical models, the eddy-rich region surrounding the Zapiola Rise (Figure 1b) leads to downslope transport of potential vorticity, associated with an upslope mass transport. This convergence generates a high pressure dome which induces a geostrophic circulation (Dewar, 1998). Bottom drag controls the flow. The convergent mass transport is compensated by a divergent Ekman transport in the bottom boundary layer (de Miranda et al., 1999; Volkov & Fu, 2008). Using numerical simulations, Weijer et al. (2015, 2020) showed that this secondary circulation leads to a strong downward vertical transport (of about 4 Sv) above the rise and they estimated a time of water mass retention of 1.5 years within the ZAC. Using satellite altimetry data, several studies pointed out the high variability of the ZAC at different time scales; intraseasonal modes of variability with periods of 20–25 days have been described by Fu et al. (2001), Weijer et al. (2007), Hughes et al. (2007) and Yu et al. (2018). Strong interannual variability has been evidenced by Fu et al. (2001), Volkov and Fu. (2008), Saraceno et al. (2009) and Venaille et al. (2011). Occasional collapses of the ZAC circulation have been suggested (Bigorre, 2005; Saraceno et al., 2009).

To the west of the Basin, a maximum of EKE centered at 40°S (with values exceeding $0.2\text{ m}^2\text{ s}^{-2}$, Figure 1b) is associated with the confluence of two strong western boundary currents: the Malvinas Current (MC) and the Brazil Current (BC) (Figure 1a). The MC which is associated with the Antarctic Circumpolar Current (ACC), flows northward following the Subantarctic Front (SAF) with surface velocities reaching 60 cm/s and a mean volume transport peaking at 37 Sv at 41°S (Artana et al., 2021). At 38°S the MC encounters the BC that flows southward (23 Sv at 36°S , Artana et al., 2021) forming the Brazil-Malvinas confluence (BMC). Those currents transport highly contrasted waters—fresh and cold for the MC, salty and warm for the BC. The BC bounded by the Subtropical Front (STF) leaves the continental slope at about 38°S , that is nearly 15° north of the zero isoline in the mean Wind Stress Curl (Figure 1c). After the collision of the two currents, a part of the BC overshoots southward to about 45°S (known as BC overshoot, BCO) before bending back to the north (Figure 1a). The MC retroflects cyclonically toward the south, flowing side by side with the BC overshoot as the Malvinas Return Flow (MRF) (Figure 1a).

Measurements being still scarce in the Argentine Basin and particularly in the Zapiola region, we take advantage of a 27-year global reanalysis from Mercator to further investigate ZAC circulation from surface to bottom and the water characteristics. After presenting the data and methods in Section 2, we examine long-term trends, multi-year modulations and extreme events of the ZAC transport (Section 3) and associated hydrographic properties (Section 4). In Section 5 we discuss the role of EKE and Wind Stress Curl in shaping those variations. In Section 6, we summarize and conclude.

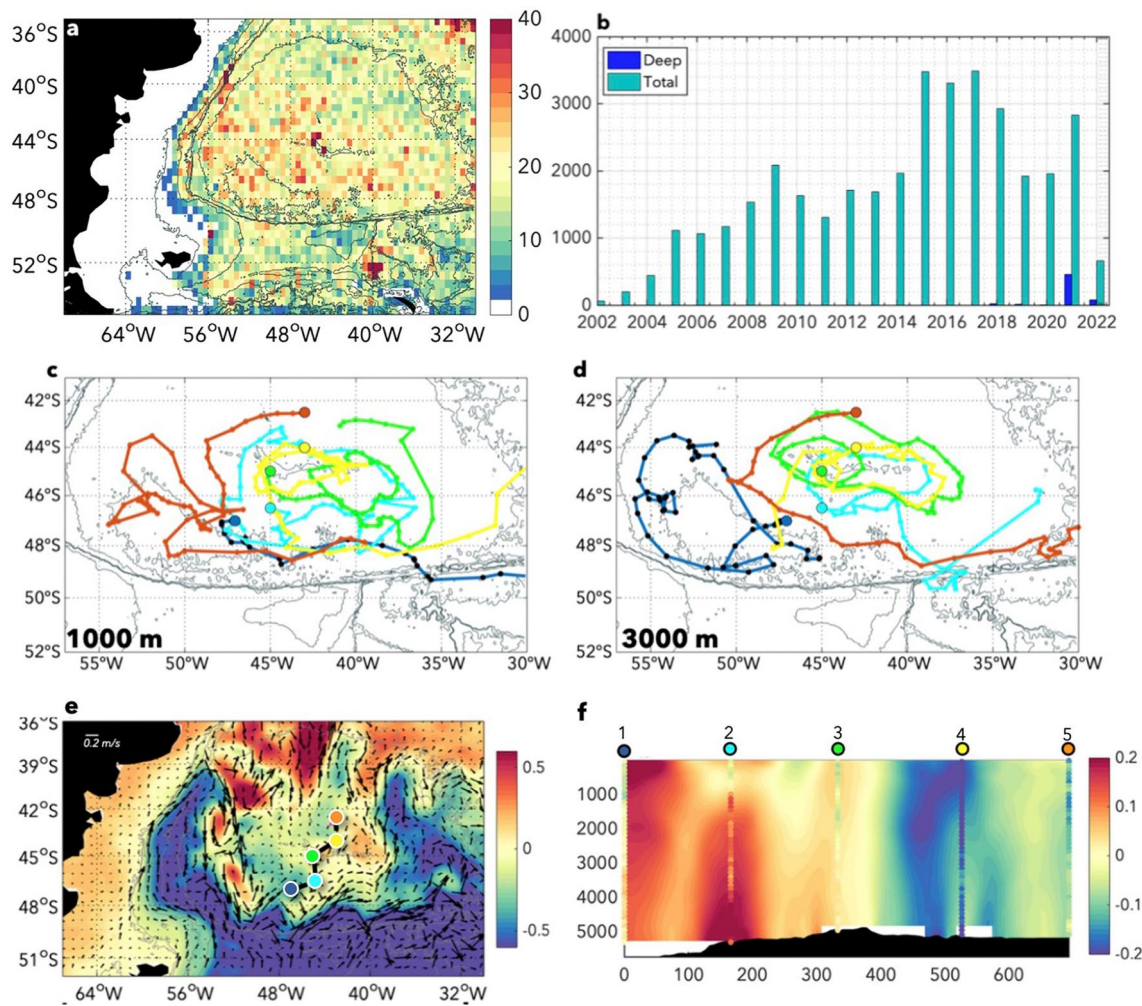


Figure 2. (a) Number of profiles per $0.5^\circ \times 0.5^\circ$ longitude-latitude bins during the period 2002–2022. (b) Total number of profiles per year in the region (cyan bars) and number of deep profiles per year in dark blue. (c) Trajectories of Argo classic floats drifting at 1,000 m (deployed in 2021, from March 12 to September 17). (d) Same as (c) for deep floats drifting at 3,000 m. (e) SSH and surface velocities from PSY4 averaged over the 12, 13 and 14 March 2021. The colored circles show the deployment locations of CTD and LADCP. (f) PSY4 zonal velocity along the dashed line in (e). LADCP zonal velocities measured at the 5 stations are represented with colored circles.

2. Operational Model and Data

2.1. Mercator Models

We used the high-resolution global Mercator Ocean reanalysis (hereafter GLORYS12) and the real-time global high-resolution forecasting system (hereafter PSY4) from Copernicus Marine Environment Monitoring Service (CMEMS, <http://marine.copernicus.eu/>; see Lellouche et al., 2021 for GLORYS12, and Lellouche et al., 2018 for PSY4). GLORYS12 covers the period from 1993 to 2019 and PSY4 from 2007 to present. The dynamical core of GLORYS12 and PSY4 is the NEMO (Nucleus for European Modeling of the Ocean) platform (Madec, 2008). The models provide daily outputs, with a horizontal resolution of $1/12^\circ$ and 50 vertical levels, with the spacing increasing with depth (22 levels are within the first 100 m leading to a vertical resolution of 1 m in the upper levels and 450 m at 5,000 m depth). Both models are forced by surface atmospheric fields from the European Center for Medium-Range Weather Forecasts (by ERA-Interim reanalysis for GLORYS12 and by the Integrated Forecasting System (IFS) for PSY4). The models assimilate along-track satellite altimetry data, satellite sea surface temperature, sea-ice concentration, and in-situ temperature and salinity profiles using a reduced-order Kalman filter with a 3-D multivariate modal decomposition of the background error and a 7-day assimilation cycle (Lellouche et al., 2018, 2021). One important impact of data assimilation is to counter the tendency of ocean models to drift

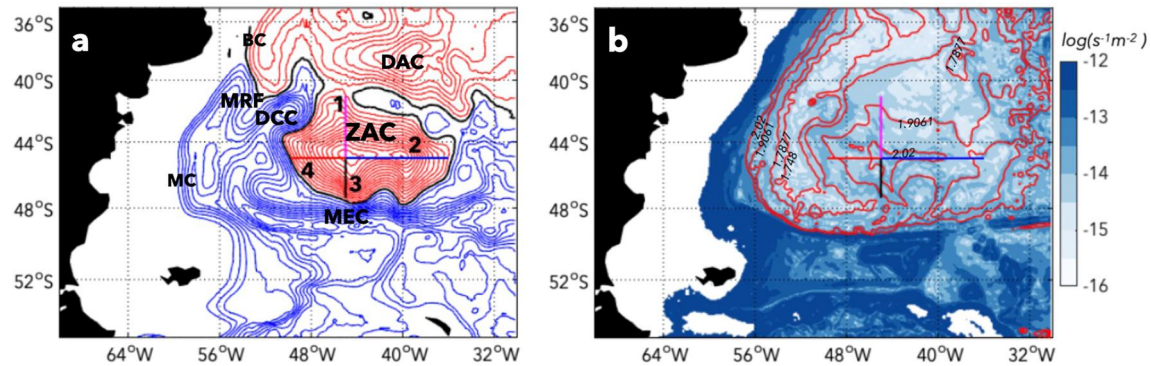


Figure 3. (a) Vertically integrated mean transport stream function computed from GLORYS12 reanalysis for the period 1993–2019 (contours every 10 Sv). Blue contours represent cyclonic and red anticyclonic circulation. The zero contour is in black. (b) \log_{10} of the modulus of f/h gradient (blue shading) and f/h contours (1.748×10^{-8} , 1.7877×10^{-8} , 1.9061×10^{-8} , $2.020 \times 10^{-8} \text{ m}^{-1} \text{ s}^{-1}$) in red. The meridional (1 and 3) and zonal (4 and 2) sections used to compute volume transports are indicated with magenta, black, red and blue lines. Acronyms in panel a stands for: MC: Malvinas Current; MRF: Malvinas Return Flow; DCC: Deep Cyclonic Circulation; ZAC: Zapiola Anticyclonic Circulation; BC: Brazil Current; DAC: Deep Anticyclonic Circulation; MEC: Malvinas Escarpment Current.

away from reality. Reanalyses provide a dynamically coherent four dimensional physical state of the ocean (temperature, salinity, velocities).

2.2. Argo Floats

The Argo program was launched in the early 2000 to provide temperature and salinity profiles in the first 2,000 m of the World Ocean using free drifting profilers (Argo float data and metadata from Global Data Assembly Centre (GDAC)). Between 2002 and present, 36,536 quality-checked profiles were obtained in the Argentine Basin (Figure 2a). After 2020, a few deep Argo floats provided data from 4,000 m up to the surface (570 profiles, Figure 2b).

Five pairs of Argo floats were deployed within the ZAC during the SAGA10W cruise on board of the Spanish R/V Sarmiento de Gamboa between the 12 and 14 of March 2021. Each pair comprised a classic float drifting at 1,000 m and a deep float drifting at 3,000 m and sampling down to 4,000 m. The Argo floats profiled to the surface every 5 days during 6 months (period of the trajectories shown in Figures 2c and 2d). CTD and LADCP measurements were performed at the deployment locations (stations shown in Figures 2c, 2e and 2f).

Mercator models assimilate observations from the Argo array in the first 2,000 m of the water column. Deep Argo floats are independent data as they are not at all assimilated in the model, which makes possible further model assessment at depth.

2.3. Further Model Validation

Previous works have already assessed the skills of global reanalysis in the first 2,000 m of the Argentine Basin with a focus on the Malvinas Current region (e.g., Artana et al., 2018, 2019; Poli et al., 2020). Here, we expand the area to 30°W and we extend in time until the end of 2021. To assess models performances at depth, we compared PSY4 model fields to data from the cruise SAGA10W and deep Argo floats deployed in 2021 (period not covered in GLORYS12) (Figure S1 in Supporting Information S1). The mean temperature and salinity (vertically averaged over bins of 400 m) and the standard deviation from model and Argo float data are close (Figures S1b and S1c in Supporting Information S1). The differences between in-situ and modeled mean salinity remain lower than 0.01 PSS-78, while below 1,200 m the modeled temperatures are slightly colder than measured ones by about 0.1° C (standard deviation of about 0.3°C) (Figures S1d, S1e and Table S1 in Supporting Information S1).

We compared PSY4 velocities to those estimated from Argo floats drifting at parking depth using the ANDRO method (Ollitrault & Rannou, 2013) which assumes that the trajectory between two successive float positions is linear (Figures 2c and 2d, see Figure S2a in Supporting Information S1). Model velocities were interpolated at the mid position between two successive Argo profiles and averaged over the elapsed time (5 days, Figure S2b in Supporting Information S1).

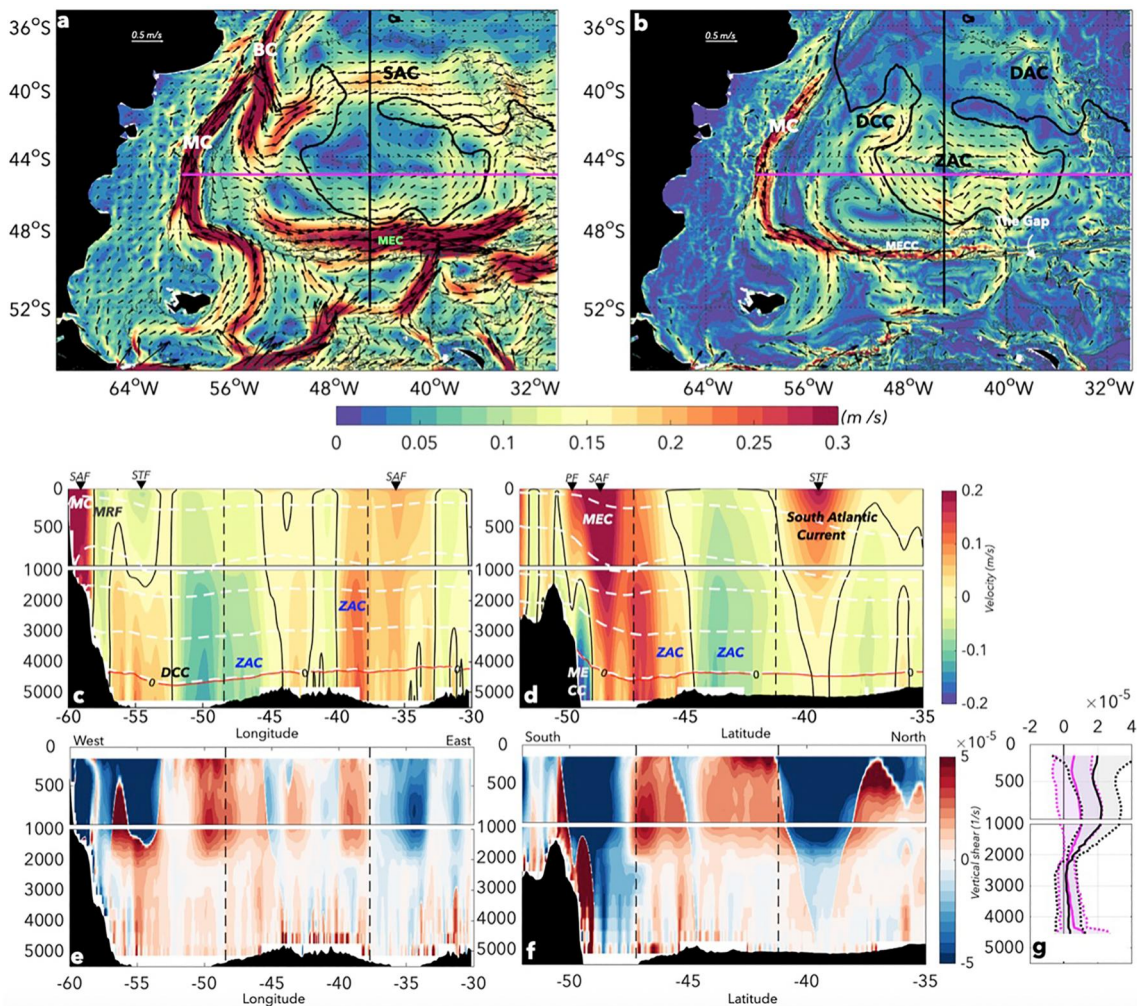


Figure 4. (a) Mean surface velocities (amplitude in color) from GLORYS12 reanalysis (1993–2019). Only velocities exceeding 0.05 m/s are plotted. The thick black isoline corresponds to the zero of the mean vertically integrated transport in Figure 3a). (b) Same as (a) for the mean velocity near the bottom, thus variable depths. (c) and (d) Mean velocities along 45°S and 45°W sections indicated in Figure 1a. White dashed lines are γ'' water masses limits (see Table S2 in Supporting Information S1). The black line corresponds to the zero velocity isoline. ZAC: Zapiola Anticyclone Circulation. MEC: Malvinas Escarpment Current; MC: Malvinas Current; MRF: Malvinas Return Flow. MECC: Malvinas Escarpment Counter Current. The mean locations of the fronts are indicated. PF: Polar Front; SAF: Subantarctic Front; STF: Subtropical Front; DCC: deep cyclonic circulation; DAC: Deep Anticyclonic Circulation. (e) and (f) Mean vertical shear of velocities interpolated every 100 m depth. (g) Mean vertical shear of velocities averaged within the ZAC and associated spatial standard deviation (shaded) along the zonal (in magenta) and meridional (in black) sections. The two vertical dashed lines correspond to the ZAC boundaries. Vertical scale is expanded in the upper 1,000 m.

Within the ZAC, differences at 1,000 and 3,000 m between the modeled and “Argo” velocities do not exceed 0.1 m/s. Outside, differences can reach 0.2 m/s, because of the strong mesoscale activity which probably limits the validity of the linear interpolation (Figures 1b–1d, Figure S3 in Supporting Information S1). Zonal velocities from PSY4 and LADCP data at the floats deployment show common patterns. For instance, both feature strong eastward velocities at depth (>0.2 m/s) above the Zapiola Rise at station 2 and strong westward velocities at station 4 (Figure 2f). Overall, the comparisons show that the model correctly reproduces hydrography and circulation of the Zapiola Anticyclone at depth.

3. Circulation in the Argentine Basin

3.1. Mean Depth-Integrated Large Scale Circulation

The vertically integrated mean transport stream function (Figure 3a) computed from the 27 years reanalysis GLORYS12 highlights structures with virtually no signature in mean surface velocities (Figure 1a). In particular the ZAC, with small surface velocities compared to other currents (Figure 4a), stands out with a mean volume

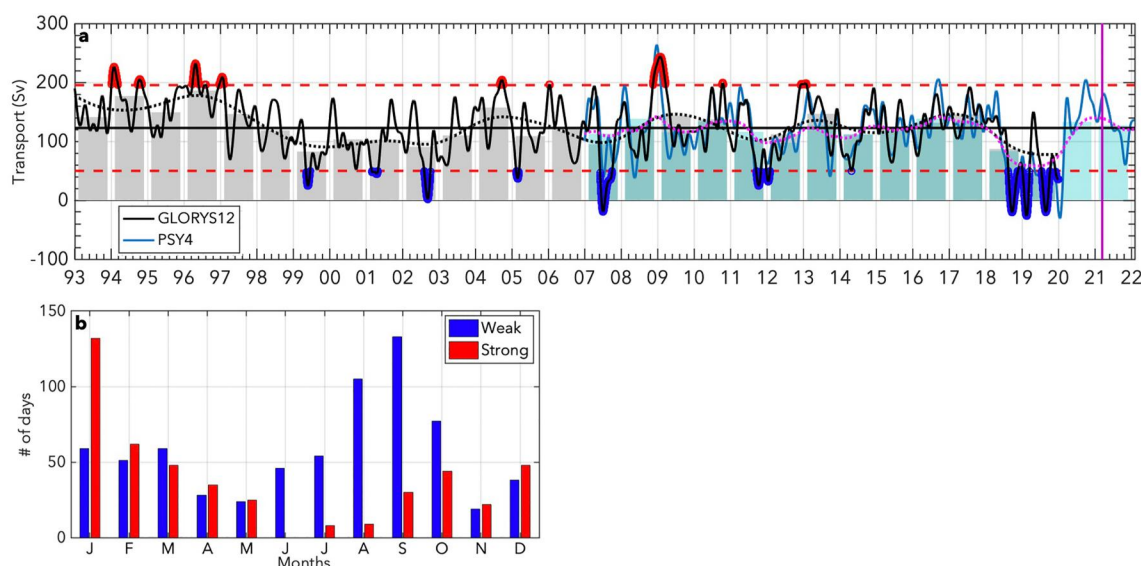


Figure 5. (a) Mean transport time series computed as explained in Section 3.2. The black horizontal line represents the mean, the red dashed lines are mean ± 1.5 standard deviation. The dashed black line shows the low-pass filtered transport (3-year cut-off period). Strong and weak events are highlighted in red and blue. The purple vertical line indicates the date of the SAGA 10W cruise. Bar plot in the background shows the annual mean of transport in gray for GLORYS12 and in blue for PSY4. (b) Monthly distribution of extreme events in number of days.

transport of 120 Sv (Figure 3a). The transport stream function closely follows f/h contours around the Zapiola Rise (Figure 3b). The two closed contours in the transport stream function around 45°S – 45°W and 45°S – 39°W correspond to two summits of the Zapiola Rise. The ZAC is intensified at depth with bottom speeds of the order of 0.10 m/s (Figure 4b). The mean cross-section speeds increase in the upper layers with a positive shear above 1,000 m ($1 \times 10^{-5} \text{ s}^{-1}$, 10 cm/s every 1,000 m, positive meaning increasing speeds with depth) while they are rather homogeneous below (small shear) (Figures 4c–4g).

Saraceno et al. (2009) estimated a mean ZAC transport of 48 Sv over the period 1993–2007 whereas we obtain 122.6 Sv over the same period. They assumed that the flow was barotropic (zero vertical shear) and used the surface geostrophic velocities derived from altimetry to compute the total transport. This method led to an underestimation of the transport as the ZAC is bottom-intensified. Colin de Verdière and Ollitrault (2016) evaluated the transport from Argo float drift velocities at 1,000 m combined with a mean oceanic climatology to compute geostrophic velocities and obtained a mean value of 124 Sv over the period 2004–2010. This value is in agreement with our estimate of 127 Sv over the same period. The reanalysis-derived value corresponds to the one estimated by Johnson and King (2023).

The total transport stream function also shows a strong cyclonic circulation centered at 42°S – 50°W , northwest of the ZAC and just east of the BC overshoot (labeled DCC for Deep Cyclonic Circulation, Figure 3a). This cyclonic circulation has almost no surface signature (Figure 1a). It transports approximately 60 Sv and follows f/h contours (see contour $1.748 \times 10^{-8} \text{ m}^{-1} \text{ s}^{-1}$ in Figure 4). Close to the bottom, velocities in the DCC reach ~ 0.2 m/s (Figure 4b). The DCC is a deep western boundary current which carries waters entering the basin through a gap located at 40°W – 48.5°S to the north east of the Malvinas Plateau (the gap is indicated in Figure 4b). These waters flow westward within a narrow current reaching 1,200 m, the Malvinas Escarpment Counter Current (hereafter MECC), which follows the Malvinas Escarpment with a mean speed around 0.2 m/s (Figures 4b–4d). Those values are consistent with direct measurements (Whitworth et al., 1991). The currents forming the DCC are in opposite direction to the surface Malvinas Escarpment Current (MEC, Figures 4a–4c at 50°S) and to the Malvinas Return Flow (MRF, Figures 4a–4c at 55°W). The mean vertical shear along the Malvinas Escarpment changes sign with depth: it is negative in the upper 2,000 m indicating a surface intensified flow and positive below with a bottom intensified flow around 50°S (Figures 4e and 4f). The differences between the upper 2,000 m and below 2,000 m could be partially related to the lack of assimilated data below 2,000 m. Model-derived vertically integrated transports of the western boundary currents (40 Sv for the northward barotropic equivalent MC at 38°S and 30 Sv for the southward BC at 36°S) agree with the

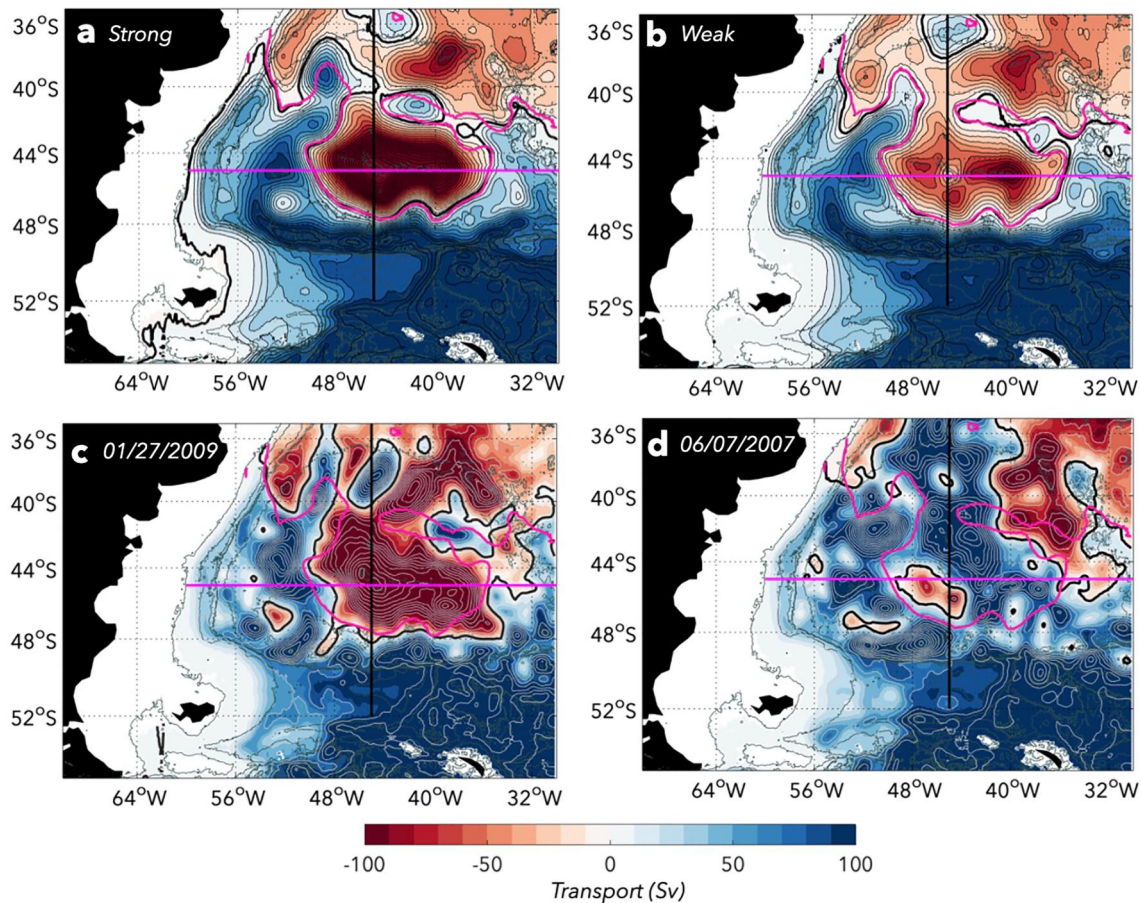


Figure 6. (a) Total transport stream function composite for strong events. Contours are plotted every 10 Sv; the 0 Sv contour is a thick black contour. The mean 0 Sv contour is in magenta from Figure 3a. (b) same as (a) for weak events. (c) and (d) Total transport stream function the 01/27/2009 (c) and the 06/07/2007 (d). Contours every 20 Sv. Black thick contours correspond to 0 Sv.

estimates from observations (Artana et al., 2018; Spadone & Provost, 2009; Maamataiaihutaipu et al., 1998; Schmid Majumder, 2018). The closed contours centered at 38°S–38°W (Figure 3a) indicate a deep anticyclonic circulation of about 50 Sv (hereafter DAC) which follows closed flh contours (Figure 3b) with bottom velocities of about 0.1 m/s (Figure 4b). The deep circulation patterns reproduced by the reanalysis are consistent with the existing literature (e.g., Whitworth et al., 1991; Peterson, 1992; Coles et al., 1994).

3.2. Variations of Low-Passed (>90 days) ZAC Transport

Four sections with a common origin at 45°S–45°W (Sections 1–4 in Figure 3) were selected to compute a time series of the ZAC volume transport. Sections 2–4 extend to the zero contour obtained from the mean total transport stream function around the Zapiola Rise and Section 1 extends to the local minimum at 41.2°S–45°W (see Figure 3a). The volume transport across zonal Sections 2 and 4 (meridional Sections 1 and 3) is defined as: $\int_0^L \int_0^H V dx dz$ ($\int_0^L \int_0^H U dy dz$) where V is the meridional component and U the zonal component of the velocity, L the section length and H the oceanic depth. A fourth-order Butterworth low-pass filter (with a cut-off frequency of 1/90 days) is applied to the transport time series corresponding to the four sections and the correlations between the four low-passed time series always exceed 0.8 (at lag 0). The four low-passed time series were averaged to obtain a unique series. We used GLORYS12 outputs for the period 1993–2019 and PSY4 outputs for 2007–2021. Transports computed from PSY4 and GLORYS12 over the overlapping period (2007–2019) show close means (115.7 and 122.6 Sv, respectively) and similar fluctuations (standard deviations of 48 and 48.5 Sv, respectively) with a correlation coefficient of 0.81 (Figure 5a).

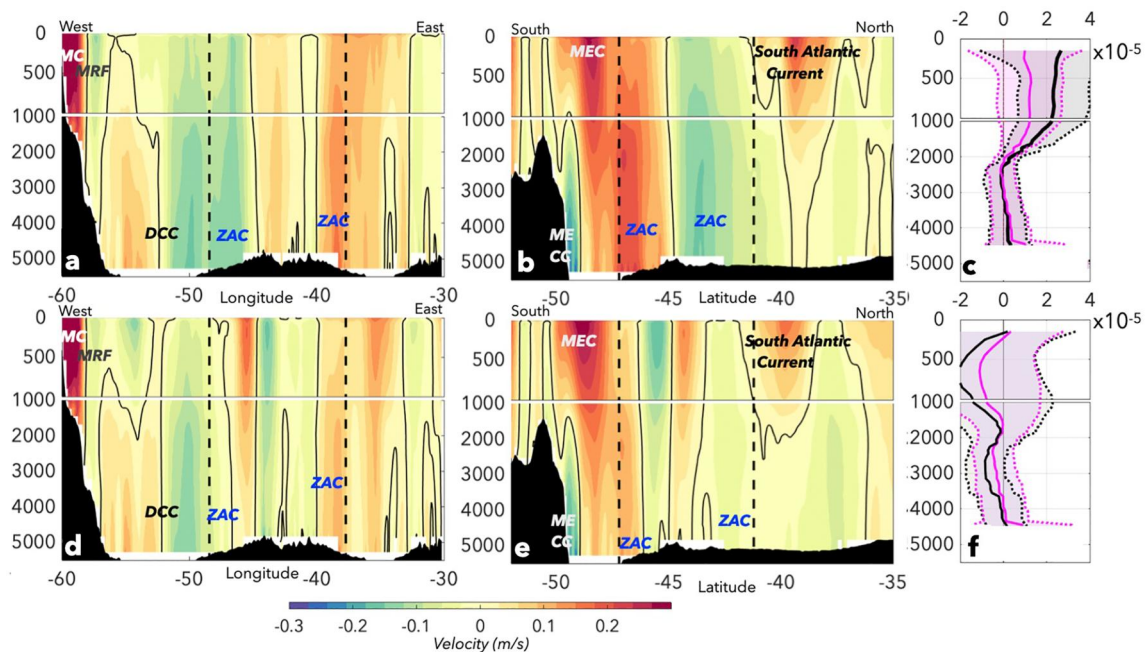


Figure 7. (a) and (b) Cross-section velocities composites along Sections 45°S (a) and 45°W (b) for strong events. The mean ZAC limits are indicated in black dashed lines. (c) Vertical velocity shear averaged within the ZAC limits for strong events and associated spatial standard deviation (shaded) along the 45°S zonal (in magenta) and 45°W meridional (in black) sections. (d)–(f) Same as (a)–(c) for weak events.

The low-pass volume transport time series includes extreme events exceeding 1.5 standard deviation (highlighted in red and blue in Figure 5) with 494 days (5% of the time series) of strong extreme events (transport exceeding 195.4 Sv, Figures 5a and 6d) and 689 days (7% of the time series) of weak extreme events (transport less than 49.8 Sv, Figures 5a and 6e). The total transport exhibits negative peaks in 2007, 2018 and 2019. The mean duration of extreme events, regardless of whether strong or weak, is approximately 65 days except for the extreme weak event of 2018–2019 which lasts 285 days. The extreme events show a seasonal distribution: weak events tend to occur in austral winter while strong events are more frequent in summer (Figure 5b).

The transport time series also features milder fluctuations over a wide range of periods between 100 and 730 days (see Figure S4 in Supporting Information S1). The annual means (gray bars) show a low frequency modulation with alternating periods of large (1993–1996, 2003–2017, 2021–2022) and low transport (1997–2003, 2018–2020) as illustrated with the black dashed line corresponding to the 3 years low passed filtered transport (Figure 5). The transport time series exhibits a robust trend of $-15 \text{ Sv.decade}^{-1}$ whatever the chosen end-point (end of 2019 or 2017 to avoid any bias due to the outstanding 2018–2019 event). The negative transport trend results from the cyclonic velocity trend pattern in the whole water column observed in the ZAC (see Figure S5 in Supporting Information S1).

3.3. The Argentine Basin During Extreme Events

To investigate the ZAC circulation and structure associated with extreme events, we computed cross-section velocities (Figure 7) and composites of the total transport stream function (Figure 6). Two specific synoptic events, the strongest event in January 2009 (with a transport reaching 268 Sv, Figure 6c) and the weak event in June 2007 (with a negative transport of -12 Sv , Figure 6d) are presented as examples.

The composites suggest that there is a little variation in the lateral extension of the ZAC during extreme events, which is consistent with a topographic influence on the circulation (Figures 6a and 6b). However, the circulation in the ZAC interior is modified. During strong events (mean transport of 211 Sv, Figure 6a), the ZAC exhibits a near solid-body rotation. The composite of weak events (mean transport of 22 Sv) shows that the ZAC includes secondary anticyclonic circulations (Figure 6b). In some occasions, like during the extreme event in January 2009

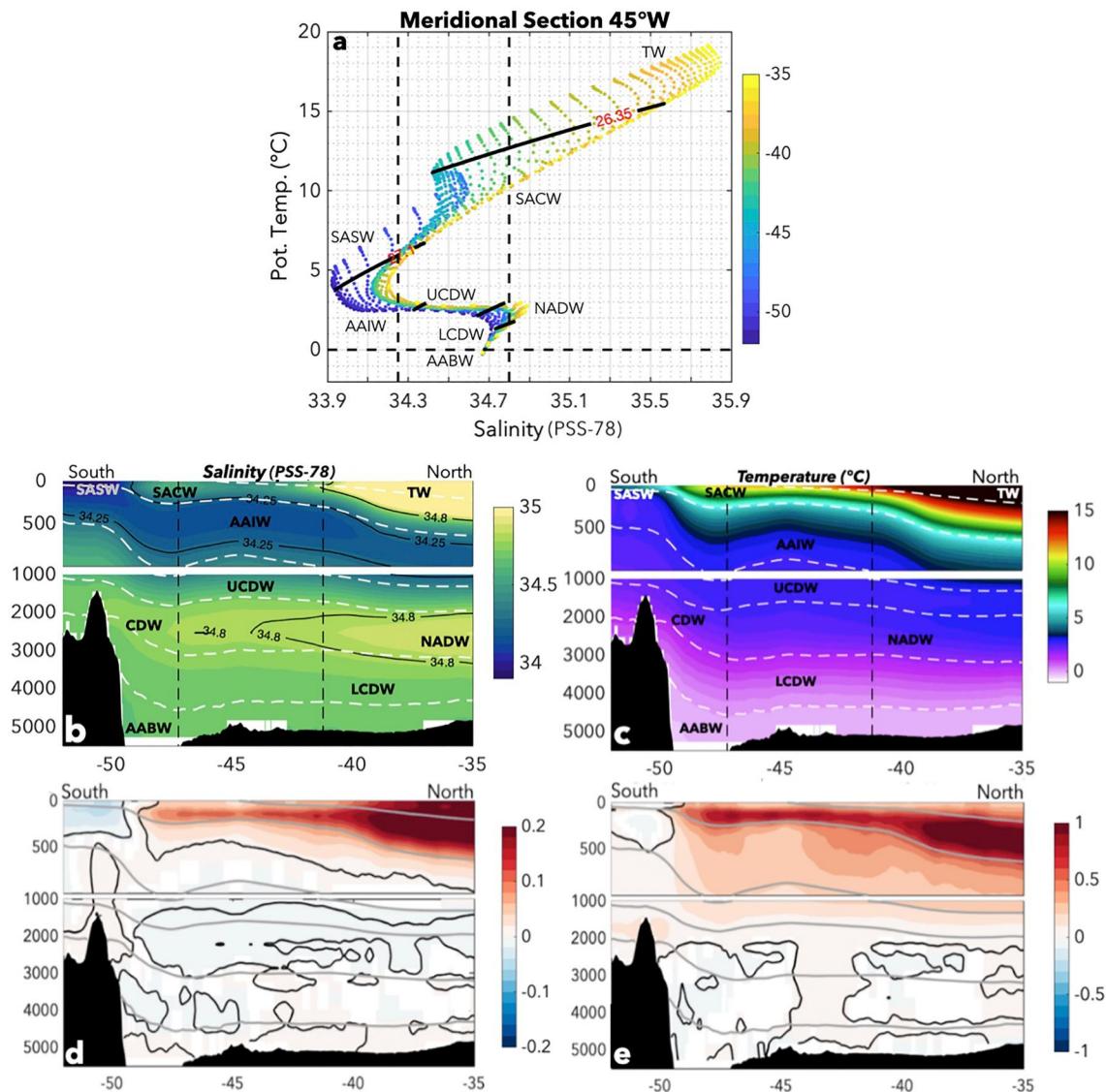


Figure 8. (a) Mean θ/S diagram along the 45°W section (black line in Figure 1a). Colors indicate latitude. γ^{ρ} contours in black mark the limits between water masses and dotted black lines the θ and S criteria of 0°C and 34.8, 34.25 PSS-78. Main water masses are labeled. (b)-(c) Mean salinity (b) and mean temperature (c) along the 45°W section as a function of latitude and depth. γ^{ρ} limits are plotted in white dashed lines, salinity criteria in black. (d) Salinity linear trends in PSS-78. decade^{-1} along the 45°W section. Shaded values are statistically significant. (e) Same as (d) for temperature in $^\circ\text{C}.\text{decade}^{-1}$. γ^{ρ} limits are plotted in thick gray lines. Thick black lines indicate regions where the absolute value of the trend exceeds the interannual standard deviation.

(268 Sv), the ZAC boundary is distorted (Figure 6c), while in June 2007 (-12 Sv), the ZAC is totally disaggregated and the overall anticyclonic circulation is disrupted (Figure 6d).

During strong events, velocities increase in the whole water column in the ZAC (Figures 7a and 7b). The velocity shear is increased between 0 and 2,000 m (compare to Figure 4g). It nearly vanishes between 2,000 and 4,500 m. This illustrates that the velocity increase is more pronounced below 2,000 m than in the upper layers. During weak events, the anticyclonic secondary circulations mentioned above are observed in the first 1,000 m of the zonal section at 45°S (Figure 7d). Below 1,500 m, outer branches of the ZAC are strongly reduced with bottom velocities less than 0.05 m/s. A cyclonic circulation with velocities reaching 0.1 m/s at the center of the ZAC is located over a depression between the two summits of the Zapiola rise (Figures 7d and 7e). The currents within the cyclonic eddy decrease with depth and the section-averaged vertical shear becomes negative in the whole water column (Figure 7f).

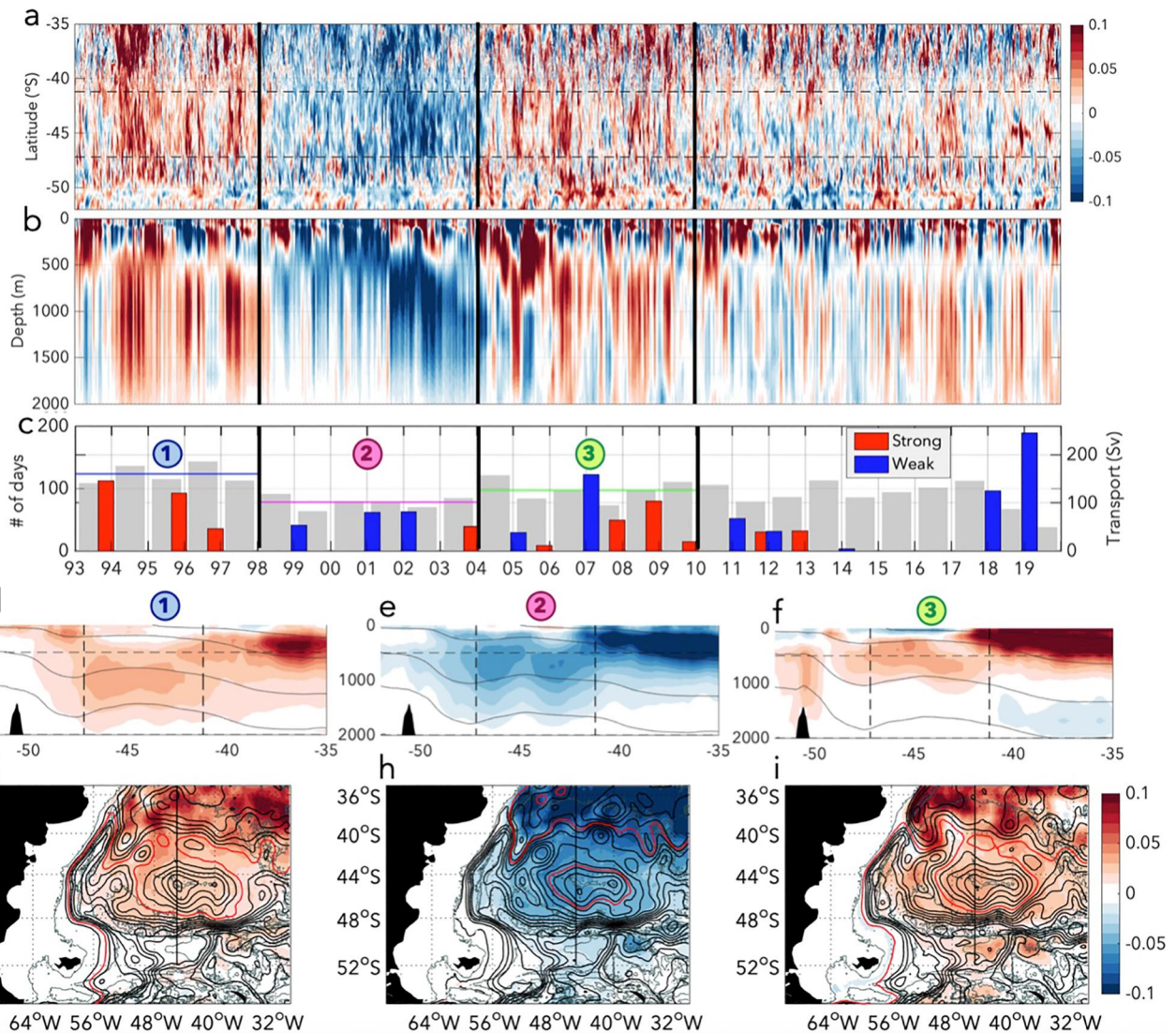


Figure 9. (a) Time-latitude diagram of detrended salinity anomalies along the 45°W section. Anomalies have been averaged between 500 and 2,000 m. Black dashed lines at 41.2° and 47.2°S correspond to the ZAC limits. (b) Time-depth diagram of detrended salinity anomalies within the ZAC. Anomalies have been averaged within the ZAC limits in the zonal and meridional direction at each depth. (c) Annual mean transport (gray bars) and yearly distribution of extreme events (red: strong events; blue: weak events). The vertical black lines separate the periods 1993–1997, 1998–2003 and 2004–2009. (d)–(f) Detrended salinity anomalies along the meridional section averaged over the periods 1993–1997 (d) 1998–2003 (e) 2004–2009 (f). Black contours correspond to neutral density limits, vertical dashed lines to the ZAC limits and horizontal black dashed lines to the 541 m depth. (g)–(i) Detrended salinity anomalies at 541 m for the three periods. Contours correspond to the transport (in Sv) integrated between 0 and 2,000 m. The red contour corresponds to the 0 Sv contour of the transport stream function and contours are every 10 Sv.

The circulation is also modified in the whole Argentine Basin during extreme events (Figure 6). The DCC is reinforced with bottom velocities reaching 0.15 m/s during strong events and weakened during weak events (Figures 7a–7c). Westward velocities associated with the MECC are above their mean values (0.2 m/s compared to 0.1 m/s) during strong events and below during weak events (−0.05 m/s). The MECC extends from the bottom up to 1,000 m depth during weak events instead of 1,300 m during strong events (1,200 m corresponds to the mean field, see Figures 6c–6g in comparison with Figure 4d).

The overall intensification or weakening of the circulation during strong and weak events suggests a large scale forcing (Figures 6 and 3a).

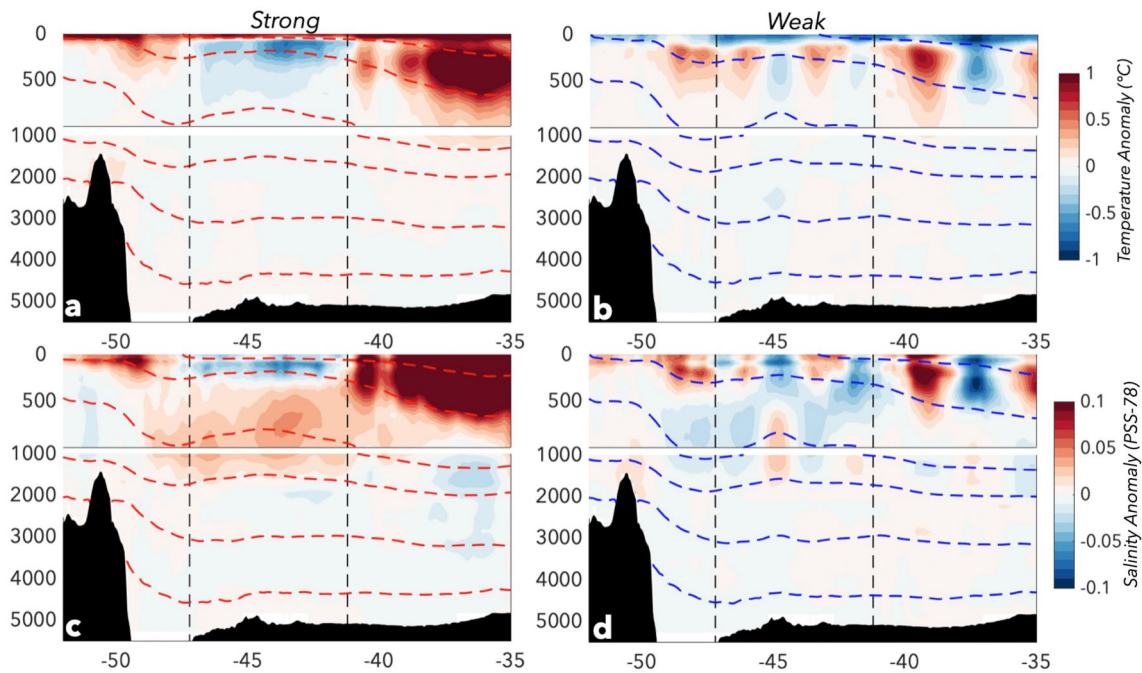


Figure 10. (a) and (b) Composite of detrended temperature anomalies for strong (a) and weak (b) events. (c) and (d) Composite of detrended salinity anomalies for strong (c) and weak (d) events. Red and blue dashed lines correspond to neutral densities and black vertical dashed lines to the ZAC limits.

4. Hydrographic Properties in the Argentine Basin

4.1. Mean and Trends in Hydrographic Properties

Water masses were identified using neutral density and salinity criteria, following Preu et al. (2013), Valla et al. (2018) and Emery and Meincke (1986) (Table S2 in Supporting Information S1). Mean hydrographic properties are illustrated along the meridional section at 45°W (Figure 8). Surface waters comprise Subantarctic Surface Waters (SASW; $\gamma^n < 27.1$ g/kg) in the first 100 m of the water column to the south of 48°S, South Atlantic Central Waters (SACW; $\gamma^n < 27.1$ g/kg) between 48°S and 42°S and Tropical Waters (TW; $\gamma^n < 26.35$ g/kg) in the upper 250 m to the north of 42°S (Figures 8a–8c). Underneath, waters are stacked as follows: Antarctic Intermediate Waters (AAIW; $27.1 < \gamma^n < 27.6$ g/kg; $33.9 < \text{salinity} < 34.25$ PSS-78), Upper Circumpolar Deep Waters (UCDW; $27.6 < \gamma^n < 27.9$ g/kg), Lower Circumpolar Deep Water (LCDW; $28.1 < \gamma^n < 28.27$ g/kg; salinity < 34.8 PSS-78) and at the bottom the Antarctic Bottom Waters (AABW; $\gamma^n > 28.27$ g/kg and negative potential temperature) (Figures 8a–8c). In the northern part of the basin, the North Atlantic Deep Waters (NADW; $27.9 < \gamma^n < 28.1$ g/kg; salinity > 34.8) lie between the UCDW and the Lower Circumpolar Deep Water (Figures 8a–8c). The Zapiola circulation induces a doming of isopycnals which are tilted at the boundaries of the ZAC (Figures 8b and 8c). Hydrographic properties exhibit trends over the 27 years-long reanalysis. We consider the trend to be significant when it is statistically significant (t -test) and when it exceeds the interannual standard deviation. Negative salinity trends close to the surface in the south of the section (-0.03 PSS-78.decade $^{-1}$, Figure 8d) are consistent with the overall freshening of subantarctic waters reported in several studies (e.g., Böning et al., 2008; Naveira Garabato et al., 2009; Purich, 2018). This freshening is significant in the MC and to the south of the ZAC (Figure S6b in Supporting Information S1). Large positive trends are observed down to 500 m in salinity ($+0.2$ PSS-78.decade $^{-1}$) and down to 1,000 m in temperature ($+1$ °C.decade $^{-1}$) to the north of the 45°W section (Figures 8d and 8e). These positive trends are significant in the whole Argentine Basin (Figure S6c in Supporting Information S1) and are probably associated with the temperature and salinity increases observed in the tropical waters in latitudes dominated by evaporation (Durack et al., 2012; Yu et al., 2020). In the ZAC the positive trend in temperature extends down to 5,000 m, which is consistent with several studies that documented bottom water warming in the Argentine Basin (e.g., Coles et al., 1996; Johnson, 2022). On top of these linear trends, water properties experienced interannual variations which are investigated in the next section.

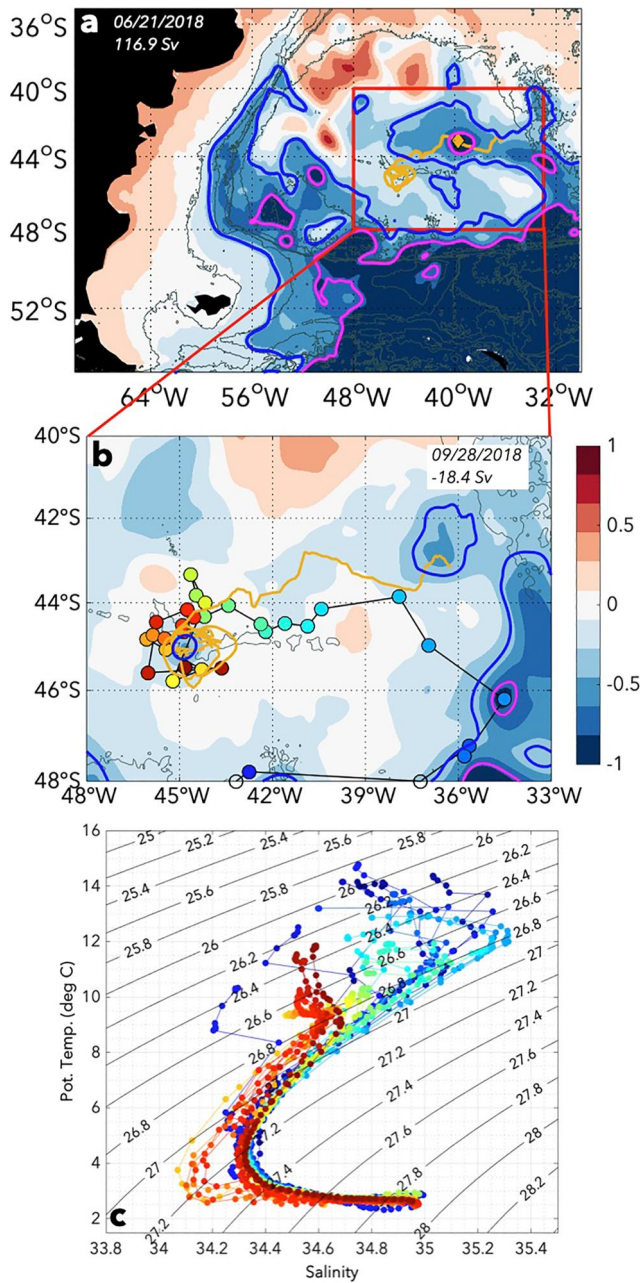


Figure 11. (a) and (b) SSH snapshots during the detachment of C1 from the SAF meander (a) the 06/21/2018 and (b) a zoom on the 09/28/2018. The eddy trajectory computed from the eddy atlas is indicated in yellow. The eddy position at the date is indicated by a yellow diamond in (a) and by a blue circle in (b). Trajectory of the Argo float #3901515 (colored dots) and C1 trajectory from the eddy atlas (yellow line). (c) θ/S diagram from Argo float #3901515 measurements. The colors correspond to the dots in panel (b).

to the ZAC intensification) on the vertical stacking of water masses. Thus there is a cold signal in the upper 700 m, a fresh signal in the upper 300 m and a salty signal between 300 and 1,500 m (Figures 10a–10c). In contrast, during weak events, the ZAC is more permeable to mesoscale structures coming from the basin, leading to temperature and salinity anomalies of opposite sign within the ZAC. The positive temperature anomalies observed between 42° S and 47° S in the 50–250 m layer (Figures 10b–10d) correspond to warm and salty waters in the secondary circulations visible in Figures 7d and 7e. These secondary anticyclonic recirculations induce a

4.2. Hydrographic Multi-Year Modulation

Linear trends were removed to investigate the interannual variability of the hydrographic characteristics. Large multi-year modulation of salinity stands out until 2010 while fluctuations of higher frequency and smaller amplitude are later observed (Figures 9a and 9b). Salinity anomalies are positive (between ≈ 0.05 and ≈ 0.1 PSS-78) and larger than the annual trend (< 0.02 PSS-78/year) during periods 1993–1997 and 2003–2009; while they are negative (between -0.05 and -0.1 PSS-78) during period 1998–2003 and extend down to 2,000 m (Figures 9a and 9b). Salinity anomalies averaged over each period along the meridional section are large to the north of 40°S in the upper 500 m (Figures 9d and 9f). Maps of averaged salinity anomalies at 541 m show a consistent large-scale signal all over the basin for each period, with the largest anomalies located within the Subtropical Gyre (Figures 9g–9i).

These distinct periods of negative (1998–2003) and positive (1993–1997 and 2004–2009) salinity anomalies coincide with weak and strong ZAC transports respectively (160 Sv for 1993–1997, 126 Sv for 2004–2009 and 101.3 Sv for 1998–2003, Figure 9c). During 1998–2003, the subtropical front (red line in Figure 9h) is shifted northward (as the transport of the Subtropical Gyre is smaller), reducing the southward advection of salty subtropical waters which could partly contribute to the salinity reduction.

The annual distribution of extreme events is not homogeneous over time. The first period accounts for a total of 240 days of strong events and no weak events, the second hosts a great majority of weak events (166 days of weak and only 39 of strong transport events). The number of weak and strong events in the third period is relatively well balanced (192 days of strong and 151 days of weak events). The last period, 2010–2019 is dominated by weak events (371 days) compared to strong events (62 days).

In the following section, we analyze the hydrographic characteristics of the ZAC during extreme events, keeping in mind their uneven temporal distribution.

4.3. Hydrographic Properties During Extreme Events

Composites of temperature and salinity anomalies for weak and strong events were compared along the 45°W section (Figure 10). Main hydrographic differences between strong and weak events are located between the surface and the UCDW (Figure 10). The signal observed in the upper 50 m reflects the seasonal distribution of weak and strong events. Weak events tend to occur in austral winter and are associated to a cold surface signal while strong events are more frequent in austral summer and are associated to a warm surface signal (Figure 5b).

During strong events the Subtropical Gyre and the MEC are intensified (cf. Section 3.2) which probably leads to the positive salinity anomalies observed to the south and north of the ZAC (Figures 10a–10c). During strong events temperature and salinity anomalies are homogeneous within the ZAC and their vertical distribution reflects the effect of the isopycnal doming (related

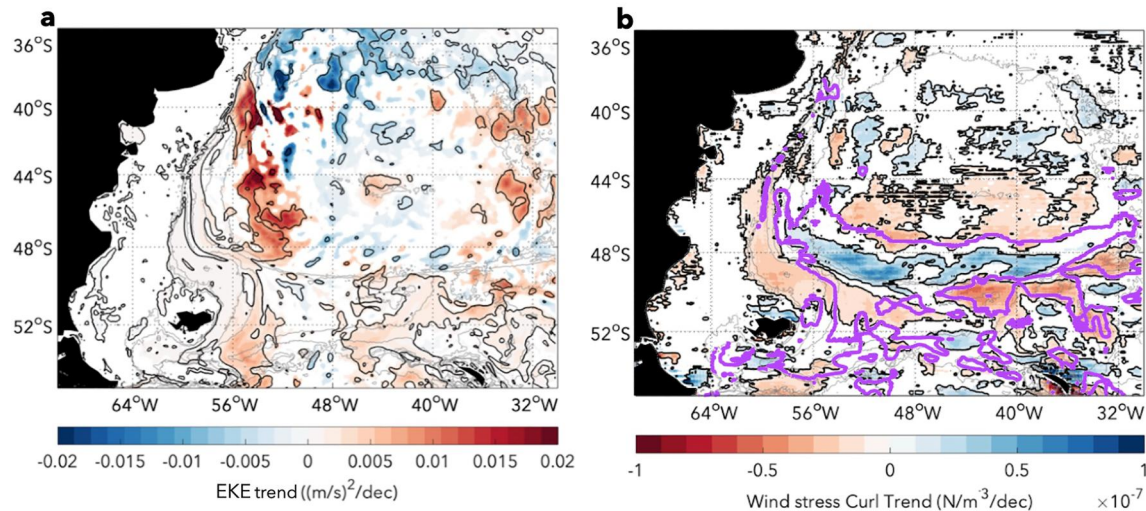


Figure 12. Linear trend over the period 1993–2019 from GLORYS12 and ERA-interim. Statistically significant values are shaded. (a) Surface EKE trend. (b) WSC trend. The thick black lines indicate regions where the absolute value of the trend exceeds the interannual standard deviation. The purple contour corresponds to the mean zero wind stress curl.

downwelling and deepening of isopycnals. A distinct isopycnal shoaling at 45°S (of about 300 m at 1,000 m, blue dashed lines in Figures 10b–10d) associated with cold (−0.3°C) and salty (+0.03 PSS-78) anomalies below 500 m correspond to the cyclonic circulation present during weak events. Every single selected weak event features a cyclonic eddy at the center of the ZAC (not shown). One of them was documented by the Argo float #3901515, which got trapped within a cyclonic eddy (C1) from October 2018 until January 2019 at the time of a drastic transport reduction (−18.5 Sv, the minimum of the transport time series) (Figure 11b). C1 lasted for more than 285 days and was tracked back in satellite maps. C1 was shed at 33°W–44°S by a meander of the SAF and the PF (on 12 May 2018) and penetrated the ZAC through the northeast boundary where the flh gradient is relatively weak (Figure 3b). It reached the center of the ZAC on the fifth August 2018 (Figures 11a and 11b). The Argo float sampled relatively cold and fresh waters within the cyclonic eddy (Figure 11c).

5. Discussion

Theoretical studies based on realistic and idealized simulations without data assimilation (e.g., Bigorre & Dewar, 2009; de Miranda et al., 1999; Venaille et al., 2011) and observational studies (e.g., Fu, 2007) suggested that the ZAC variability is driven by kinetic energy transfers and wind stress curl. GLORYS12 tends to reproduce the EKE at the right time and location probably due to data assimilation. However, the precise distinction between the role of data assimilation and model dynamics is challenging. We computed the EKE as follows: $EKE = \frac{U'^2 + V'^2}{2}$ with $U' = U - \bar{U}$ and $V' = V - \bar{V}$, the overbar indicated the velocities time average over the entire period.

EKE and WSC exhibit trends over 27 years that emerge from interannual variability (Figure 12).

The linear trend of surface EKE is negative to the north of 40°S (−0.015 (m/s)².decade^{−1}) and positive to the south (+0.015 (m/s)².decade^{−1}), reflecting the southward shift of the BC (strong anticyclonic trend in the surface velocities of the BCO, see Figure S5 in Supporting Information S1) and the entire Subtropical Gyre. This EKE trend is consistent with the global increase in mesoscale activity documented at the poleward boundaries of the Subtropical Gyres over the satellite altimetry record (e.g., Martinez-Moreno et al., 2021; Li et al., 2023). The WSC linear trends are positive over the central Argentine Basin and negative along the Malvinas Escarpment and of the same sign of the mean WSC (Figure 1c), depicting an overall intensification of the atmospheric circulation (Figure 12b). The trends are consistent with the intensification and expansion, toward the West and the South, of the South Atlantic anticyclone that has been documented over the last decades (e.g., Leyba et al., 2019; Li et al., 2023).

We opted for a composite analysis to examine EKE and WSC signals associated to extreme events as correlations between the EKE and the transport (WSC and the transport) were non conclusive as the system is strongly non linear.

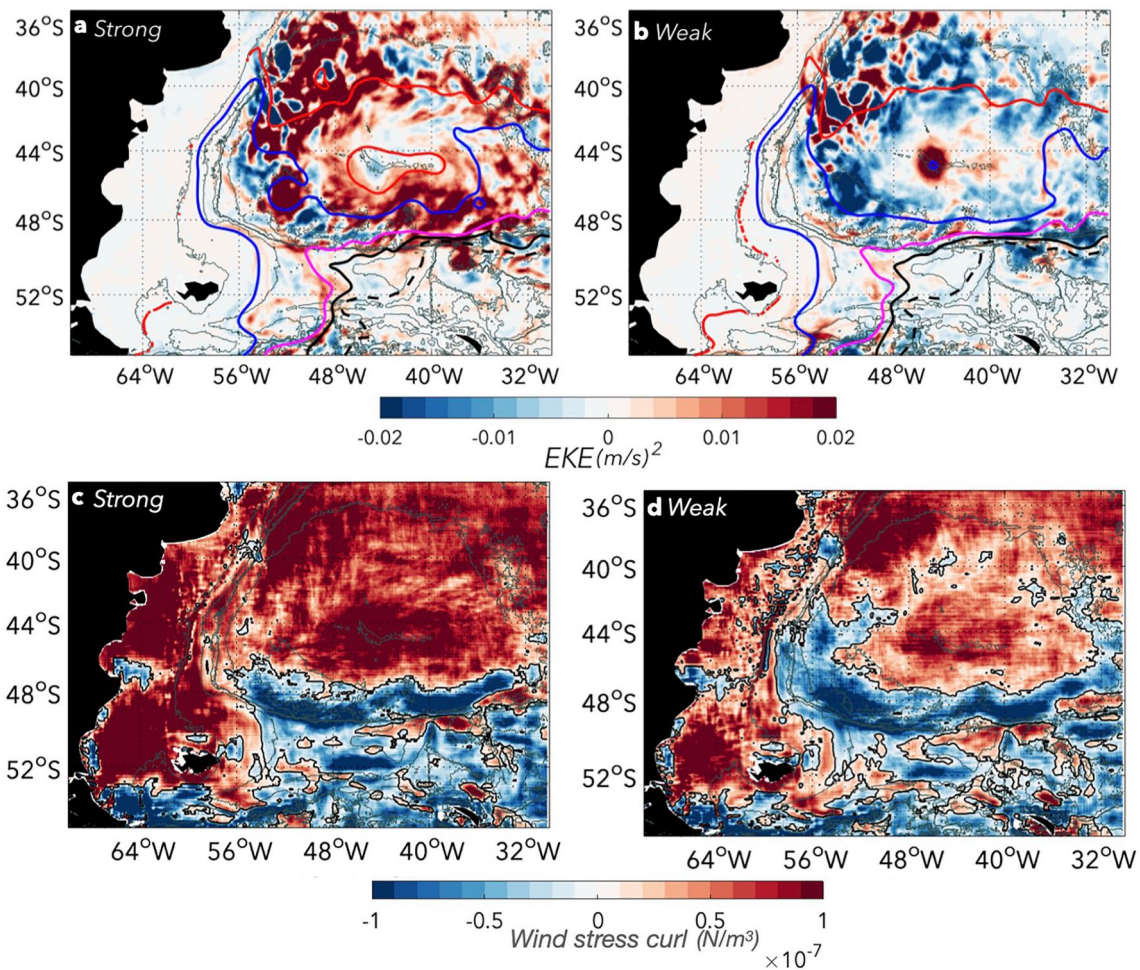


Figure 13. (a) and (b) Composite of surface EKE anomalies for strong (a) and weak (b) events. Thick colored contours in panels indicate the position of the fronts (STF in red, SAF in blue and PF in magenta and black). (c) and (d) Wind Stress Curl composites for (c) strong and (d) weak events. The zero Wind Stress Curl line is in black.

Composites of detrended EKE anomalies for weak and strong events exhibit similar patterns but of opposite sign. Overall, the basin exhibits an increase of EKE during strong events except at the center of the ZAC while the opposite occurs during weak events. The EKE increase at the center of the ZAC during weak events reflects the cyclonic circulation previously described (see Sections 3 and 4.3). Conversely, the EKE is enhanced at the boundaries of the ZAC and reduced close to the center during strong events: the inward penetration of eddies is inhibited.

During strong events the WSC is enhanced over the ZAC and the southern part of the Subtropical Gyre, reinforcing the negative Ekman suction in those regions while the opposite occurs during weak events. This is consistent with the large-scale current intensification described in Section 3.3 (Figure 6). The mean position of the zero WSC isoline in the western part of the basin is located southward around 48°S during strong events and northward around 41°S during weak events.

As extreme events present a seasonal distribution (Figure 5b), we explored the seasonal means of EKE and WSC (Figure 14). The seasonal averages of EKE show similar patterns the extreme events EKE composites (although smaller values) with more energy to the north of the confluence in summer (strong events) than in winter (weak events). This signal is probably associated with the summer southward shift of the subtropical front (Figures 13a and 13b). The WSC is reinforced during austral summer and weakened in winter (Figures 13c and 13d) and resembles to the composite in terms of spatial pattern and magnitude. Wind Seasonal variability could favor the development of extreme transport events and their persistence. However, causality is not established.

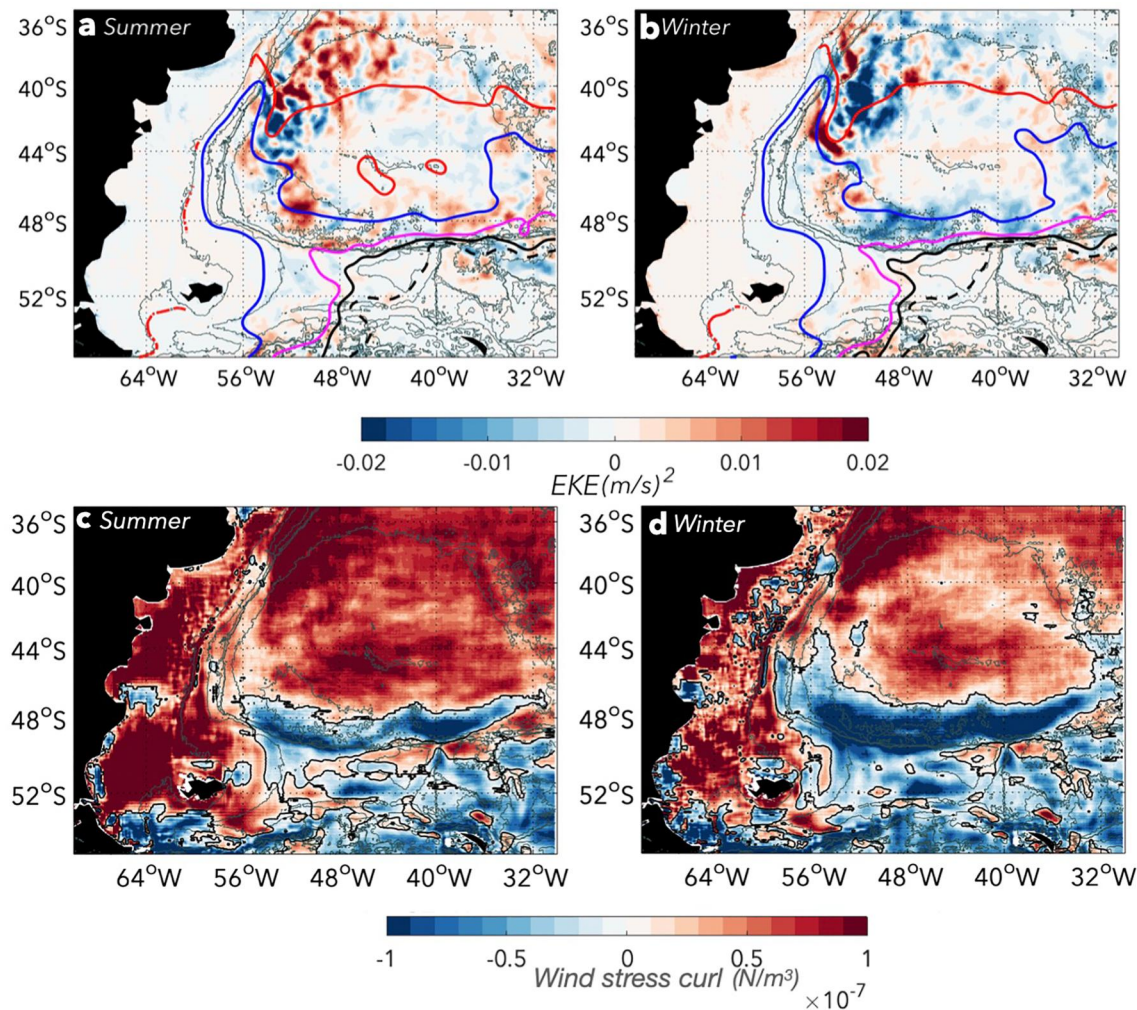


Figure 14. (a) and (b) Seasonal detrended surface EKE anomalies averaged for DJF (a) and JJA (b). (c) Mean summer (DJF) detrended Wind Stress Curl. (d) Mean winter detrended (JJA) Wind Stress Curl.

6. Summary and Concluding Remarks

We used a global ocean reanalysis (GLORYS12) over the period 1993–2019 to investigate the ZAC. The ZAC is bottom intensified with velocities reaching 0.1 m/s which is in agreement with a recent study based on in situ observations (Johnson & King, 2023). We constructed a 27 years-long ZAC transport time series which ranges between 268 Sv and -18.4 Sv with a mean value of 122.6 Sv (standard deviation of 48.5 Sv). The transport presents a strong multi-year modulation, a robust negative trend (-15 Sv.decade $^{-1}$) and extreme events (exceeding 1.5 standard deviation, 494 days of strong events and 689 days of weak events). The number of extreme events is rather limited (only 9 strong extreme events and weak events) to perform robust statistics.

During strong events (transport >195.4 Sv), the ZAC shows a well defined coherent gyre. In contrast, during weak events (transport <49.8 Sv) secondary anticyclonic circulations develop within the ZAC and a cyclonic eddy is located at the center of the ZAC. During weak events, the ZAC is more permeable to external mesoscale structures. Each weak event features a cyclonic eddy at the center of the ZAC carrying cold and fresh waters. These eddies detach from a SAF meander to the east of the ZAC and enter through the north-east boundary where the planetary vorticity gradient is relatively weak. Strong events are associated with an increase of EKE around the ZAC while weak events are associated with a decrease. As suggested in theoretical studies (e.g., Bigorre & Dewar, 2009) the increase of EKE could lead to an enhanced transfer of energy between the mesoscale field and the mean flow.

During strong events the WSC intensifies over the ZAC possibly enhancing the negative Ekman suction (reverse is true for weak events) (Figures 13c and 13d). The mean seasonal patterns of WSC resemble those of the composites of extrema suggesting that the WSC seasonality could favor the development of extreme events (Figures 14c and 14d). However, this is a speculative hypothesis, as the similarity between the strong/weak composites of WSC in Figures 13c and 13d and the summer/winter seasonal averages in Figures 14c and 14d could simply reflect the seasonal bias in occurrence of strong/weak events and causality is not established.

We documented a multi-year modulation of the water masses characteristics in the ZAC. Waters in the ZAC are fresher (-0.75 PSS-78 at 1,000 m) and colder (-0.5°C at 1,000 m) in the period 1998–2003 than in periods 1993–1997 and 2004–2009. The period 1998–2003 corresponds to a reduced mean transport of 101.3 Sv compared to the other periods (160 Sv over 1993–1997 and 126 Sv over 2004–2009). The weak transport period corresponds to a reduction of the large scale circulation (including the Subtropical Gyre) associated to weaker winds and EKE. This period (1998–2003) includes only weak events.

Over the last 27 years, transport time series exhibits a significant negative trend of -15 Sv.decade $^{-1}$ associated with a cyclonic velocity trend pattern in the ZAC coherent in the vertical (see Figure S5 in Supporting Information S1). The ZAC shows a positive temperature trend ($+0.5^{\circ}\text{C}$.decade $^{-1}$ at 500 m) in the whole water column, a positive salinity trend ($+0.1$.decade $^{-1}$ at 500 m) in the upper 2,000 m and a negative salinity trend between 3,000 and 4,000 m. The WSC exhibits no change over the ZAC and a positive trend at the periphery. The WSC over the South Atlantic has been shown to contribute to the southward displacement of the STF (Leyba et al., 2019). The southward migration of the Subtropical Gyre induces a negative EKE trend to the northwest of the ZAC and a positive trend to the south of 40°S close to the MC. The negative EKE trend could be a factor leading to the ZAC transport reduction. Anticyclones detaching from the BCO and transporting relatively warm and salty waters could contribute to the positive trends in salinity and temperature within the ZAC in the first 2,000 m. Indeed, the ZAC gets more permeable to the surrounding mesoscale features as it weakens (positive trend of EKE at the center of the ZAC).

Climate models project a continuous southward migration of the Subtropical Gyre (e.g., Hewitt et al., 2020) which will increase temperature and salinity in the Argentine Basin. Associated EKE changes could contribute to a reduction of the ZAC transport and a multiplication of collapses episodes.

Conflict of Interest

The authors declare no conflicts of interest relevant to this study.

Data Availability Statement

Model outputs are available at Copernicus Marine Environment Monitoring Service (CMEMS; <https://marine.copernicus.eu>). ERA-Interim outputs are available at <https://www.ecmwf.int/en/forecasts/datasets/reanalysis-datasets/era-interim>. The Argo data used in this study were download from an Argo Global Data Assembly Center in May 2023 (Argo, 2023).

References

- Argo (2023). Argo float data and metadata from Global Data Assembly Centre (Argo GDAC). [Dataset]. <https://doi.org/10.17882/42182.SEANOE>
- Artana, C., Lellouche, J.-M., Park, Y.-H., Garric, G., Koenig, Z., Sennéchaël, N., et al. (2018). Fronts of the Malvinas Current System: Surface and subsurface expressions revealed by satellite altimetry, Argo floats, and Mercator operational model outputs. *Journal of Geophysical Research: Oceans*, 123(8), 5261–5285. <https://doi.org/10.1029/2018JC013887>
- Artana, C., Provost, C., Lellouche, J.-M., Rio, M.-H., Ferrari, R., & Sennéchaël, N. (2019). The Malvinas current at the confluence with the Brazil current: Inferences from 25 years of Mercator Ocean reanalysis. *Journal of Geophysical Research: Oceans*, 124(10), 7178–7200. <https://doi.org/10.1029/2019JC015289>
- Artana, C., Provost, C., Poli, L., Ferrari, R., & Lellouche, J.-M. (2021). Revisiting the Malvinas Current upper circulation and water masses using a high-resolution ocean reanalysis. *Journal of Geophysical Research: Oceans*, 126(6), e2021JC017271. <https://doi.org/10.1029/2021JC017271>
- Bigorre, S. (2005). *Topographic effects on wind driven oceanic circulation*. (Ph.D. Thesis), Florida State University, (pp. 100). Retrieved from <http://etd.lib.fsu.edu/theses/available/etd-07052005-163825/unrestricted/pro-dis2E.pdf>
- Bigorre, S., & Dewar, W. K. (2009). Oceanic time variability near a large scale topographic circulation. *Ocean Modelling*, 29(3), 176–188. <https://doi.org/10.1016/j.ocemod.2009.04.004>
- Böning, C., Dispert, A., Visbeck, M., Rintoul, S. R., & Schwarzkopf, F. U. (2008). The response of the Antarctic Circumpolar Current to recent climate change. *Nature Geoscience*, 1(12), 864–869. <https://doi.org/10.1038/ngeo362>

Acknowledgments

We warmly thank Josep Luis Pelegrí (ICM, Barcelona), Alonso Hernandez-Guerra (IOCAG, ULPGC), Mikhail Emelianov (ICM, Barcelona), the crew and science parties of the R/V Sarmiento de Gamboa for measurements and Deep Argo float deployment assistance in the Argentine Basin. We are grateful to CNES (Centre National d'Etudes Spatiales) for constant support. This study is a contribution to the CNES-funded BACI project and to the LEFE GMMC BACI project. Léa Poli acknowledges Ph.D support from Sorbonne Université and Camila Artana funding from the Spanish government (AEI) through the "Severo Ochoa Centre of Excellence" accreditation (CEX2019-000928-S). We thank the editor, Léon Chafik, an anonymous reviewer, and Wilbert Weijer for a number of constructive comments and suggestions.

- Coles, V. J., McCartney, M. S., Olson, D. B., & Smethie, W. M. (1996). Changes in Antarctic bottom water properties in the western South Atlantic in the late 1980s. *Journal of Geophysical Research: Oceans*, *101*(C4), 8957–8970. <https://doi.org/10.1029/95jc03721>
- Colin de Verdière, A. C., & Ollitrault, M. (2016). A direct determination of the World Ocean barotropic circulation. *Journal of Physical Oceanography*, *46*(1), 255–273. <https://doi.org/10.1175/JPO-D-15-0046.1>
- de Miranda, A. P., Barnier, B., & Dewar, W. K. (1999). On the dynamics of the Zapiola Anticyclone. *Journal of Geophysical Research: Oceans*, *104*(C9), 21137–21149. <https://doi.org/10.1029/1999jc900042>
- Dewar, W. K. (1998). Topography and barotropic transport control by bottom friction. *Journal of Marine Research*, *56*(2), 295–328. <https://doi.org/10.1357/002224098321822320>
- Durack, P. J., Wijffels, S. E., & Matear, R. J. (2012). Ocean salinities reveal strong global water cycle intensification during 1950 to 2000. *Science*, *336*(6080), 455–458. <https://doi.org/10.1126/science.1212222>
- Emery, W. J., & Meincke, J. (1986). Global water masses—summary and review. *Oceanologica Acta*, *9*(4), 383–391.
- Flood, R. D., & Shor, A. N. (1988). Mud waves in the Argentine Basin and their relationship to regional bottom circulation patterns. *Deep Sea Research Part A: Oceanographic Research*, *35*(6), 943–971. [https://doi.org/10.1016/0198-0149\(88\)90070-2](https://doi.org/10.1016/0198-0149(88)90070-2)
- Fu, L. L. (2007). Interaction of mesoscale variability with large-scale waves in the Argentine Basin. *Journal of Physical Oceanography*, *37*(3), 787–793. <https://doi.org/10.1175/jpo2991.1>
- Fu, L.-L., Cheng, B., & Qiu, B. (2001). 25-Day period large-scale oscillations in the Argentine Basin revealed by the TOPEX/Poseidon altimeter. *Journal of Physical Oceanography*, *31*(2), 506–517. [https://doi.org/10.1175/1520-0485\(2001\)031<0506:DPLSOI>2.0.CO;2](https://doi.org/10.1175/1520-0485(2001)031<0506:DPLSOI>2.0.CO;2)
- Hewitt, H. T., Roberts, M., Mathiot, P., Biastoch, A., Blockley, E., Chassignet, E. P., et al. (2020). Resolving and parameterising the Ocean mesoscale in earth system models. *Current Climate Change Reports*, *6*(4), 137–152. <https://doi.org/10.1007/s40641-020-00164-w>
- Hughes, C. W., Stepanov, V. N., Fu, L. L., Barnier, B., & Hargreaves, G. W. (2007). Three forms of variability in Argentine Basin ocean bottom pressure. *Journal of Geophysical Research*, *112*(C1). <https://doi.org/10.1029/2006jc003679>
- Johnson, G. C. (2022). Antarctic bottom water warming and circulation slowdown in the Argentine Basin from analyses of deep Argo and historical shipboard temperature data. *Geophysical Research Letters*, *49*(18), e2022GL100526. <https://doi.org/10.1029/2022GL100526>
- Johnson, G. C., & King, B. A. (2023). Zapiola Gyre, velocities and mixing, new Argo insights. *Journal of Geophysical Research: Oceans*, *128*(6), e2023JC019893. <https://doi.org/10.1029/2023JC019893>
- Lellouche, J.-M., Greiner, E., Le Galloudec, O., Garric, G., Regnier, C., Drevillon, M., et al. (2018). Recent updates to the Copernicus Marine Service global ocean monitoring and forecasting real-time 112° high-resolution system. *Ocean Science*, *14*(5), 1093–1126. <https://doi.org/10.5194/os-14-1093-2018>
- Lellouche, J.-M., Greiner, E., Romain, B.-B., Gilles, G., Angélique, M., Marie, D., et al. (2021). The Copernicus global 1/12° oceanic and sea ice GLORYS12 reanalysis. *Frontiers in Earth Science*, *9*, 698876. <https://doi.org/10.3389/feart.2021.698876>
- Leyba, I. M., Solman, S. A., & Saraceno, M. (2019). Trends in sea surface temperature and air–sea heat fluxes over the South Atlantic Ocean. *Climate Dynamics*, *53*(7–8), 4141–4153. <https://doi.org/10.1007/s00382-019-04777-2>
- Li, Q., England, M. H., Hogg, A. M., Rintoul, S. R., & Morrison, A. K. (2023). Abyssal ocean overturning slowdown and warming driven by Antarctic meltwater. *Nature*, *615*(7954), 841–847. <https://doi.org/10.1038/s41586-023-05762-w>
- Maamaatuaiahutapu, K., Garçon, V., Provost, C., & Mercier, H. (1998). Transports of the Brazil and Malvinas currents at their confluence. *Journal of Marine Research*, *56*(2), 417–438. <https://doi.org/10.1357/002224098321822366>
- Madec, G. (2008). *NEMO reference manual, ocean dynamic component: NEMO-OPA, Note du Pôle de modélisation*. In Institut Pierre Simon Laplace (No. 27). Technical Report 27, Note du pôle de modélisation. Institut Pierre Simon Laplace.
- Martínez-Moreno, J., Hogg, A. M., England, M. H., Constantinou, N. C., Kiss, A. E., & Morrison, A. K. (2021). Global changes in oceanic mesoscale currents over the satellite altimetry record. *Nature Climate Change*, *11*(5), 397–403. <https://doi.org/10.1038/s41558-021-01006-9>
- Mason, E., Pascual, A., Gaube, P., Ruiz, S., Pelegrí, J. L., & Delepuille, A. (2017). Subregional characterization of mesoscale eddies across the Brazil-Malvinas Confluence. *Journal of Geophysical Research: Oceans*, *122*(4), 3329–3357. <https://doi.org/10.1002/2016JC012611>
- Naveira Garabato, A. C., Jullion, L., Stevens, D. P., Heywood, K. J., & King, B. A. (2009). Variability of subantarctic mode water and Antarctic intermediate water in the Drake passage during the late-twentieth and early-twenty-first centuries. *Journal of Climate*, *22*(13), 3661–3688. <https://doi.org/10.1175/2009JCLI2621.1>
- Ollitrault, M., & Rannou, J.-P. (2013). ANDRO: An argo-based deep displacement dataset. *Journal of Atmospheric and Oceanic Technology*, *30*(4), 759–788. <https://doi.org/10.1175/JTECH-D-12-00073.1>
- Peterson, R. G. (1992). The boundary currents in the western Argentine Basin. *Deep Sea Research*, *39*(3–4), 623–644. [https://doi.org/10.1016/0198-0149\(92\)90092-8](https://doi.org/10.1016/0198-0149(92)90092-8)
- Poli, L., Artana, C., Provost, C., Sirven, J., Sennéchaël, N., Cuypers, Y., & Lellouche, J.-M. (2020). Anatomy of subinertial waves along the Patagonian shelf break in a 1/12° global operational model. *Journal of Geophysical Research: Oceans*, *125*(12). <https://doi.org/10.1029/2020JC016549>
- Preu, B., Hernández-Molina, F. J., Violante, R., Piola, A. R., Paterlini, C. M., Schwenk, T., et al. (2013). Morphosedimentary and hydrographic features of the northern Argentine margin: The interplay between erosive, depositional and gravitational processes and its conceptual implications. *Deep Sea Research Part I: Oceanographic Research Papers*, *75*, 157–174. <https://doi.org/10.1016/j.dsr.2012.12.013>
- Purich, A. (2018). *Understanding the drivers of recent Southern Ocean sea ice and surface temperature trends*. (Doctoral dissertation). UNSW.
- Saraceno, M., Provost, C., & Zajaczkowski, U. (2009). Long-term variation in the anticyclonic ocean circulation over the Zapiola Rise as observed by satellite altimetry: Evidence of possible collapses. *Deep Sea Research Part I: Oceanographic Research Papers*, *56*(7), 1077–1092. <https://doi.org/10.1016/j.dsr.2009.03.005>
- Saunders, P. M., & King, B. A. (1995). Bottom currents derived from a shipborne ADCP on WOCE cruise A11 in the South Atlantic. *Journal of Physical Oceanography*, *25*(3), 329–347. [https://doi.org/10.1175/1520-0485\(1995\)025<0329:bcdfas>2.0.co;2](https://doi.org/10.1175/1520-0485(1995)025<0329:bcdfas>2.0.co;2)
- Schmid, C., & Majumder, S. (2018). Transport variability of the Brazil Current from observations and a data assimilation model. *Ocean Science*, *14*(3), 417–436. <https://doi.org/10.5194/os-14-417-2018>
- Spadone, A., & Provost, C. (2009). Variations in the Malvinas current volume transport since October 1992. *Journal of Geophysical Research*, *114*(C2), C02002. <https://doi.org/10.1029/2008JC004882>
- Valla, D., Piola, A. R., Meinen, C. S., & Campos, E. (2018). Strong mixing and recirculation in the northwestern Argentine Basin. *Journal of Geophysical Research: Oceans*, *123*(7), 4624–4648. <https://doi.org/10.1029/2018jc013907>
- Venaille, A., Le Sommer, J., Molines, J.-M., & Barnier, B. (2011). Stochastic variability of oceanic flows above topography anomalies. *Geophysical Research Letters*, *38*(16), L16611. <https://doi.org/10.1029/2011GL048401>
- Volkov, D. L., & Fu, L.-L. (2008). The role of vorticity fluxes in the dynamics of the Zapiola Anticyclone. *Journal of Geophysical Research*, *113*(C11), C11015. <https://doi.org/10.1029/2008JC004841>

- Weatherly, G. (1993). On deep-current and hydrographic observations from a mudwave region and elsewhere in the Argentine Basin. *Deep Sea Research, Part II*, 40(4–5), 939–961. [https://doi.org/10.1016/0967-0645\(93\)90042-1](https://doi.org/10.1016/0967-0645(93)90042-1)
- Weijer, W., Barthel, A., Veneziani, M., & Steiner, H. (2020). The Zapiola Anticyclone: A Lagrangian study of its kinematics in an eddy-permitting ocean model. *Deep Sea Research Part I: Oceanographic Research Papers*, 164, 103308. <https://doi.org/10.1016/j.dsr.2020.103308>
- Weijer, W., Maltrud, M. E., Homoky, W. B., Polzin, K. L., & Maas, L. R. (2015). Eddy-driven sediment transport in the Argentine Basin: Is the height of the Zapiola Rise hydrodynamically controlled? *Journal of Geophysical Research: Oceans*, 120(3), 2096–2111. <https://doi.org/10.1002/2014JC010573>
- Weijer, W., Vivier, F., Gille, S. T., & Dijkstra, H. A. (2007). Multiple oscillatory modes of the Argentine Basin. Part I: Statistical analysis. *Journal of Physical Oceanography*, 37(12), 2855–2868. <https://doi.org/10.1175/2007jpo3527.1>
- Whitworth, T., III, Nowlin, W. D., Jr., Pillsbury, R. D., Moore, M. I., & Weiss, R. F. (1991). Observations of the Antarctic Circumpolar current and deep boundary current in the southwest Atlantic. *Journal of Geophysical Research*, 96(C8), 15105–15118. <https://doi.org/10.1029/91jc01319>
- Yu, L., Josey, S. A., Bingham, F. M., & Lee, T. (2020). Intensification of the global water cycle and evidence from ocean salinity: A synthesis review. *Annals of the New York Academy of Sciences*, 1472(1), 76–94. <https://doi.org/10.1111/nyas.14354>
- Yu, Y., Chao, B. F., García-García, D., & Luo, Z. (2018). Variations of the Argentine Gyre observed in the GRACE time-variable gravity and ocean altimetry measurements. *Journal of Geophysical Research: Oceans*, 123(8), 5375–5387. <https://doi.org/10.1029/2018jc014189>